Analytic energy gradient of projected Hartree-Fock within projection after variation

Uejima, Motoyuki

Ten-no, Seiichiro

(Citation)
Journal of Chemical Physics,146(10):104106-104106

(Issue Date)
2017-03-14

(Resource Type)
journal article

(Version)
Version of Record

Analytic energy gradient of projected Hartree–Fock within projection after variation

Motoyuki Uejima, and Seiichiro Ten-no

Citation: The Journal of Chemical Physics **146**, 104106 (2017);
View online: https://doi.org/10.1063/1.4978050
View Table of Contents: http://aip.scitation.org/toc/jcp/146/10
Published by the American Institute of Physics

Analytic energy gradient of projected Hartree–Fock within projection after variation

Motoyuki Uejima[1] and Seiichiro Ten-no[1,2,a)]
[1]*Graduate School of Science, Technology, and Innovation, Kobe University, Rokkodai-cho, Nada-ku, Kobe 657-8501, Japan*
[2]*Graduate School of System Informatics, Kobe University, Rokkodai-cho, Nada-ku, Kobe 657-8501, Japan*

(Received 5 January 2017; accepted 22 February 2017; published online 10 March 2017)

We develop a geometrical optimization technique for the projection-after-variation (PAV) scheme of the recently refined projected Hartree–Fock (PHF) as a fast alternative to the variation-after-projection (VAP) approach for optimizing the structures of molecules/clusters in symmetry-adapted electronic states at the mean-field computational cost. PHF handles the nondynamic correlation effects by restoring the symmetry of a broken-symmetry single reference wavefunction and moreover enables a black-box treatment of orbital selections. Using HF orbitals instead of PHF orbitals, our approach saves the computational cost for the orbital optimization, avoiding the convergence problem that sometimes emerges in the VAP scheme. We show that PAV-PHF provides geometries comparable to those of the complete active space self-consistent field and VAP-PHF for the tested systems, namely, CH_2, O_3, and the $[Cu_2O_2]^{2+}$ core, where nondynamic correlation is abundant. The proposed approach is useful for large systems mainly dominated by nondynamic correlation to find stable structures in many symmetry-adapted states. *Published by AIP Publishing.* [http://dx.doi.org/10.1063/1.4978050]

I. INTRODUCTION

One of the most fascinating and challenging themes in quantum chemistry is to enable the treatment of an electronic state with strong correlation such as an assembly of dissociating molecules and biradical species. The correlation energy, defined as the difference between the Hartree–Fock (HF) and full configuration interaction (FCI) energies, can be classified into the contributions of the dynamic and nondynamic correlation effects.

Dynamical correlation arising from instantaneous electron collisions is usually described by many excited determinants with relatively small amplitudes compared to the weight of the reference of HF wavefunction. For the ground state predominated by a single Slater determinant, a qualitative description of dynamic correlation is recovered by the use of a single-reference (SR) correlated method, e.g., many-body perturbation theory (MBPT)[1] and coupled cluster (CC) theory.[2] In contrast, the nondynamic correlation effects, arising from the degeneracy or quasi-degeneracy, can be described by employing multi-determinants of equal importance for the states. Multi-configuration self-consistent field (MCSCF)[3] is a useful means for this purpose, if an appropriate active space is chosen. The complete active space (CAS) is frequently employed for MCSCF, i.e., CASSCF.[4]

Despite the potential ability of CASSCF for describing nondynamic correlation, its applications to larger molecules and clusters are hindered by the computational cost that increases combinatorially with respect to the numbers of electrons and orbitals in the active space. The recent advances of density matrix renormalization group (DMRG)[5,6] have somewhat mitigated this situation, enabling the treatment of multinuclear transition-metal complexes.[7]

Broken-symmetry unrestricted HF (BS-UHF) and Kohn–Sham have been used more routinely for large molecules with strong correlation as these methods account for the vast amounts of nondynamic correlation at the mean-field computational costs.[8,9] A symmetry-breaking lowers the total energy because of the increase in the variational parameters. Nevertheless, the ambiguous electronic structure of such a broken-symmetry scheme often leads to qualitatively incorrect optimal geometric structures and molecular properties.

It has been well-known that the proper symmetries of a BS wavefunction can be restored by the symmetry projection prescriptions,[10–18] many cases of which are limited to the spin symmetry projection based on the projector suggested by Löwdin.[10] Since this projection operator is expressed as a product of N spin-flip excitations from a UHF wavefunction, for the number of electrons N, the resulting equation becomes extremely complicated to deal with. To relieve this difficulty, approximate truncations have been often employed. However, such truncations sometimes spoil the essence of projection, enhancing the relative weights of contaminants, that cannot be eliminated completely.

Another PHF approach with a different projection operator, that is widely used in nuclear physics, has been recently introduced in quantum chemistry by Scuseria and coworkers.[19] This approach requires much less computational cost for the exact symmetry adaptation, retaining the

a)Author to whom correspondence should be addressed. Electronic mail: tenno@garnet.kobe-u.ac.jp. Tel: +81-78-803-6125. Fax: +81-78-803-6125.

description of nondynamic correlation. Among the possible symmetry projections, the spin-projected unrestricted Hartree–Fock (SUHF), which restores spin-symmetry exactly from a single spin-unrestricted Slater determinant, is especially promising. The variational optimization of the projected determinant, viz., the VAP-SUHF scheme, has been adopted to overcome the ill behavior of spontaneous symmetry breaking originating from the transition between degenerate/nondegenerate electronic states.[19] Approaches to incorporating dynamic correlation into the PHF wavefunction and obtaining excited states have been developed in a similar manner to the post HF theories. Time-dependent projected Hartree–Fock (TD-PHF)[20] provides single electron excitation energies from a VAP wavefunction. Extended Møller–Plesset perturbation (EMP) theory[21] and extended configuration interaction single and double (ECISD)[22,23] treat the dynamic correlation missing in PHF.

For locating a stable molecular geometry in a pure spin symmetry, the use of PHF is preferable to BS-UHF or BS-KS. The analytic energy gradient of VAP-SUHF has been developed by Schutki *et al.*[24] The VAP scheme sometimes fails to converge in the self-consistent field (SCF) procedure or to find the most stable solution for large molecules with the direct inversion of iterative subspace (DIIS) procedure[25] because of the presence of small eigenvalues in the Hessian elements that often appear in SUHF. A quadratically convergent SCF appears to circumvent this difficulty at the expense of additional computational cost. Alternatively, it is expected that a qualitatively correct wavefunction can be obtained from the PAV scheme when BS-UHF captures the nondynamic correlation effects sufficiently. The PAV approach is computationally more affordable than VAP, and therefore it has an advantage in practical use for geometrical optimization. In this paper, we explore this alternative route and develop the analytic energy gradient of SUHF in the PAV scheme.

This paper is organized as follows. The derivation of the energy gradient of PAV-SUHF is presented in Section II. We also present the projection for the point group symmetry briefly. The computer implementation is discussed in detail in Section III. The PAV-SUHF geometrical optimization is applied to CH_2, O_3, and the $[Cu_2O_2]^{2+}$ core. Section IV presents the results of the PAV-SUHF in geometrical optimization compared with those of UHF, VAP-SUHF, and CASSCF. Finally, our conclusion of the PAV-SUHF optimization is provided in Section V.

II. THEORY

A. The energy expression of PHF

In order to make the current work as self-contained as possible, here we describe the PHF method. The projection of reference BS state $|\Psi\rangle$ onto the symmetry adapted (SA) state vector characterized by the quantum numbers j and m is expressed as

$$|jm\rangle = \sum_{m'} f^j_{m'} \hat{P}^j_{mm'} |\Psi\rangle, \tag{1}$$

where $\hat{P}^j_{mm'}$ denotes the projection operator for arbitrary groups. Note that $\hat{P}^j_{mm'}$ with $m \neq m'$ is not a projection operator but is often used to incorporate the missing components of degenerated states.

The projection for spin symmetry is defined by

$$\hat{P}^j_{mm'} = \frac{2j+1}{8\pi^2} \int d\omega D^{j*}_{mm'}(\omega) \hat{R}(\omega), \tag{2}$$

where $\hat{R}(\omega)$ and $D^j_{mm'}(\omega)$ respectively indicate the spin rotation operator and the Wigner matrix for spin rotation of j-spin state with the spin rotation angle ω. Since a UHF wave function is an eigenfunction of S_z with an eigenvalue m, the spin projection operator for BS-UHF can be expressed by the spin rotation only in the y-axis,

$$\hat{P}^j_{mm} = \frac{2j+1}{2} \int_0^\pi d\theta \sin\theta \, d^{j*}_{mm}(\theta) \hat{R}(\theta), \tag{3}$$

where $d^j_{mm}(\theta)$ represents the Wigner small matrix.

To restore the spatial symmetry, we also use the point group symmetry projection operator $\hat{P}^\Gamma_{\gamma\gamma'}$, where Γ denotes the irreducible representation, and γ and γ' indicate respectively row and column for the representation matrix D^Γ. The combination of the spin and point group symmetries is simply represented by $\hat{P}^j_{mm'}\hat{P}^\Gamma_{\gamma\gamma'}$. In this paper, we call this type of PHF, e.g., C_{2v}SUHF, for a molecule belonging to C_{2v}.

Defining the projected Hamiltonian $\mathbf{H}$ and overlap matrix $\mathbf{N}$,

$$H^j_{mm'} = \langle\Psi|\hat{H}\hat{P}^j_{mm'}|\Psi\rangle, \tag{4}$$

$$N^j_{mm'} = \langle\Psi|\hat{P}^j_{mm'}|\Psi\rangle, \tag{5}$$

the expectation value of projected energy E^j is obtained by solving the eigenvalue problem

$$\sum_{m'} H^j_{mm'} f^j_{m'} = E^j \sum_{m'} N^j_{mm'} f^j_{m'}. \tag{6}$$

A single determinant is assumed for the reference BS state $|\Psi\rangle$, represented by molecular orbitals (MOs)

$$|\psi_p\rangle = \sum_\mu C_{\mu p} |\mu\rangle, \tag{7}$$

where μ and $C_{\mu p}$ are atomic orbitals and spin dependent MO coefficients, respectively.

For numerical calculations, the transform regarding the continuous group is discretized as

$$\frac{2j+1}{8\pi^2} \int d\omega D^{j*}_{mm'}(\omega)\hat{R}(\omega) \approx \sum_g w_g D^{j*}_{mm'}(\hat{R}_g)\hat{R}_g. \tag{8}$$

The overlap between bare and rotated determinants is defined as

$$M_g = \langle\Psi|\hat{R}_g|\Psi\rangle, \tag{9}$$

to yield the projected Hamiltonian and norm elements

$$H^j_{mm'} = \sum_g w_g D^{j*}_{mm'}(\hat{R}_g) M_g E_g, \tag{10}$$

$$N^j_{mm'} = \sum_g w_g D^{j*}_{mm'}(\hat{R}_g) M_g. \tag{11}$$

E_g is the transition energy at each quadrature point

$$E_g = \frac{\langle\Psi|\hat{H}\hat{R}_g|\Psi\rangle}{\langle\Psi|\hat{R}_g|\Psi\rangle} = \frac{1}{2}\sum_{\mu\nu}(h_{\mu\nu} + F_{g,\mu\nu})\rho_{g,\nu\mu}, \tag{12}$$

where $\boldsymbol{\rho}_g$ is the transition density matrix between the bare and rotated determinants

$$\rho_{g,\mu\nu} = \sum_{pq}\frac{\langle\Psi|\hat{c}_q^\dagger\hat{c}_p\hat{R}_g|\Psi\rangle}{\langle\Psi|\hat{R}_g|\Psi\rangle}C_{\nu q}^* C_{\mu p}. \tag{13}$$

$h_{\mu\nu}$ and $F_{\mu\nu,g}$ stand for the matrix elements of the core Hamiltonian and transition Fock matrix, respectively. The latter is defined by

$$F_{g,\mu\nu} = h_{\mu\nu} + \sum_{\lambda\sigma}\langle\mu\lambda||\nu\sigma\rangle\rho_{g,\sigma\lambda}. \tag{14}$$

B. Energy gradient of PHF in the VAP scheme

Schutski *et al.* derived the energy gradient for a VAP wavefunction from the Lagrangian[24]

$$L^{\mathrm{VAP}}[\mathbf{f}^j, \mathbf{C}, \boldsymbol{\epsilon}] := W^{\mathrm{PHF}}[\mathbf{f}^j, \mathbf{C}] - E^j(\mathbf{f}^{j\dagger}\mathbf{N}^j\mathbf{f}^j - 1) - \sum_{pq}\epsilon_{pq}([\mathbf{C}^\dagger\mathbf{S}\mathbf{C}]_{pq} - \delta_{pq}), \tag{15}$$

by imposing the normalization condition on the state vectors,

$$\sum_{mm'} f_m^{j*} f_{m'}^j N_{mm'}^j = 1, \tag{16}$$

$$\sum_{\mu\nu} C_{\mu p}^* S_{\mu\nu} C_{\nu q} = \delta_{pq}, \tag{17}$$

where $S_{\mu\nu}$ are overlap integrals of atomic orbitals, and W^{PHF} stands for the energy functional for PHF,

$$W^{\mathrm{PHF}}[\mathbf{f}^j, \mathbf{C}] = \mathbf{f}^{j\dagger}\mathbf{H}^j\mathbf{f}^j. \tag{18}$$

The stationary condition leads to

$$\frac{\partial L^{\mathrm{VAP}}}{\partial f_{m'}^j} = \sum f_m^{j*} H_{mm'}^j - E^j\sum_m f_m^{j*} N_{mm'}^j = 0, \tag{19}$$

$$\frac{\partial L^{\mathrm{VAP}}}{\partial C_{\mu p}} = \frac{\partial W^{\mathrm{PHF}}}{\partial C_{\mu p}} - E^j\sum_{mm'} f_m^{j*} f_{m'}^j \frac{\partial N_{mm'}^j}{\partial C_{\mu p}} - [\boldsymbol{\epsilon}\mathbf{C}^\dagger\mathbf{S}]_{p\mu} = 0. \tag{20}$$

The first condition is equivalent to Eq. (6). Eq. (20) is the PHF equation that is in the matrix form,

$$\mathbf{C}^\dagger\mathbf{F}^{\mathrm{PHF}} = \boldsymbol{\epsilon}\mathbf{C}^\dagger\mathbf{S}, \tag{21}$$

where $\mathbf{F}^{\mathrm{PHF}}$ is the effective Fock matrix for PHF,[24] and all $\epsilon_{pq} = 0$ when the self-consistency is achieved. Therefore, the energy gradient for the VAP wavefunction, which does not contain ϵ_{pq}, is given by

$$\frac{dE^{j(VAP)}}{dx} = \frac{dL^{\mathrm{VAP}}}{dx} = W^{\mathrm{PHF}(x)} - E^j\mathbf{f}^{j\dagger}\mathbf{N}^{j(x)}\mathbf{f}^j. \tag{22}$$

The derivative of the energy for the PHF energy functional is

$$W^{\mathrm{PHF}(x)} = \sum_{mm'} f_m^{j*} f_{m'}^j \sum_g w_g D_{mm'}^{j*}(\hat{R}_g) M_g \times \left(E_g^{(x)} + E_g\mathrm{Tr}[\mathbf{S}^x\boldsymbol{\rho}_g] - \mathrm{Tr}[\mathbf{F}_g\boldsymbol{\rho}_g\mathbf{S}^x\boldsymbol{\rho}_g]\right), \tag{23}$$

where the superscript x represents the derivative with respect to x, and (x) means the same yet with the $C_{\mu p}$ dependence frozen. Therefore, ${E_g}^{(x)}$ is defined as

$${E_g}^{(x)} := \sum_{\mu\nu}\left[h_{\mu\nu}^x + \frac{1}{2}\sum_{\lambda\sigma}\langle\mu\lambda||\nu\sigma\rangle^x\rho_{g,\sigma\lambda}\right]\rho_{g,\nu\mu}. \tag{24}$$

The matrix product of the second term on the right side of Eq. (22) is expressed as

$$\mathbf{f}^{j\dagger}\mathbf{N}^{j(x)}\mathbf{f}^j = \sum_{mm'} f_m^{j*} f_{m'}^j \sum_g w_g D_{mm'}^{j*}(\hat{R}_g) M_g \mathrm{Tr}[\mathbf{S}^x\boldsymbol{\rho}_g]. \tag{25}$$

Therefore, the derivative of the energy for the VAP scheme is given by

$$\frac{dE^{j(\mathrm{VAP})}}{dx} = \sum_{mm'} f_m^{j*} f_{m'}^j \sum_g w_g D_{mm'}^{j*}(\hat{R}_g) M_g \times \left\{E_g^{(x)} + (E_g - E^j)\mathrm{Tr}[\mathbf{S}^x\boldsymbol{\rho}_g] - \mathrm{Tr}[\mathbf{F}_g\boldsymbol{\rho}_g\mathbf{S}^x\boldsymbol{\rho}_g]\right\}. \tag{26}$$

C. Energy gradient of PHF in the PAV scheme

Since the PAV energy does not fulfill the variational condition with respect to the orbital coefficients, the orbital dependent part $\partial\mathbf{C}/\partial x$ has to be taken into account. To this end, it is necessary to solve the coupled perturbed HF (CPHF) equation. Handy and Schaefer proposed the Z-vector technique,[26] which avoids solving the CPHF equations. We formulate the energy gradient of PAV-SUHF using this technique.

In a similar manner of Furche and Ahlrichs[27] for analytic energy gradient of TDDFT, we define the Lagrangian which becomes stationary at the convergence with respect to all parameters, $\mathbf{f}^j$, $\mathbf{C}$, $\mathbf{z}$, and $\mathbf{w}$,

$$L^{\mathrm{PAV}}[\mathbf{f}^j, \mathbf{C}, \mathbf{z}, \mathbf{w}] := W^{\mathrm{PHF}}[\mathbf{f}^j, \mathbf{C}] - E^j(\mathbf{f}^{j\dagger}\mathbf{N}^j\mathbf{f}^j - 1) + \sum_{ai}[z_{ia}\mathcal{F}_{ai}^{\mathrm{Ref}} + z_{ai}\mathcal{F}_{ia}^{\mathrm{Ref}}] - \sum_{pq} w_{qp}([\mathbf{C}^\dagger\mathbf{S}\mathbf{C}]_{pq} - \delta_{pq}), \tag{27}$$

where $\mathcal{F}_{ai}^{\mathrm{Ref}}$ and $\mathcal{F}_{ia}^{\mathrm{Ref}}$ are the occupied-virtual and virtual-occupied parts of the Fock matrix for the reference BS wavefunction, respectively. For SUHF, $\mathcal{F}^{\mathrm{Ref}}$ is the UHF Fock matrix. The Lagrangian multipliers $\mathbf{f}$, $\mathbf{z}$, and $\mathbf{w}$ fulfill the conditions

$$\frac{\partial L^{\mathrm{PAV}}}{\partial f_{m'}^j} = \sum f_m^{j*} H_{mm'}^j - E^j\sum_m f_m^{j*} N_{mm'}^j = 0, \tag{28}$$

$$\frac{\partial L^{\mathrm{PAV}}}{\partial z_{ai}} = \mathcal{F}_{ai}^{\mathrm{Ref}} = \mathcal{F}_{ia}^{\mathrm{Ref}} = 0, \tag{29}$$

$$\frac{\partial L^{\mathrm{PAV}}}{\partial w_{pq}} = [\mathbf{C}^\dagger\mathbf{S}\mathbf{C}]_{pq} - \delta_{pq} = 0, \tag{30}$$

where (28) again corresponds to Eqs. (6) and (29) is the Brillouin condition. The Lagrangian derivatives with respect to the transpose of the multipliers are also null. The multipliers $\mathbf{z}$ and $\mathbf{w}$ are determined from the stationary condition with respect to the MO coefficients,

$$\frac{\partial L^{\mathrm{PAV}}}{\partial C_{\mu p}} = \frac{\partial L^{\mathrm{PAV}}}{\partial C_{\mu p}^*} = 0, \tag{31}$$

resulting in the equations for $\mathbf{z}$,

$$\begin{aligned}(\epsilon_i^{\mathrm{Ref}} - \epsilon_a^{\mathrm{Ref}})z_{ia} &= \mathcal{F}_{ia}^{\mathrm{PHF}} + \sum_{bj}(z_{jb}\langle bi||ja\rangle + z_{bj}\langle ji||ba\rangle),\\ (\epsilon_i^{\mathrm{Ref}} - \epsilon_a^{\mathrm{Ref}})z_{ai} &= \mathcal{F}_{ai}^{\mathrm{PHF}} + \sum_{bj}(z_{jb}\langle ba||ji\rangle + z_{bj}\langle ja||bi\rangle),\end{aligned} \tag{32}$$

and for $\mathbf{w}$,

$$\begin{aligned}w_{ij} &= \sum_{ak} z_{ak}\langle ki||aj\rangle + \sum_{ak} z_{ka}\langle ai||kj\rangle,\\ w_{ai} &= z_{ai}\epsilon_i^{\mathrm{Ref}}, \qquad w_{ia} = z_{ia}\epsilon_i^{\mathrm{Ref}}, \qquad w_{ab} = 0.\end{aligned} \tag{33}$$

Eq. (32) is the so-called Z-vector equation. We obtain $\mathbf{z}$ order-by-order for $\mathbf{z}^{(n)}$ as

$$\begin{aligned}z_{ai}^{(0)} &= 0,\\ z_{ai}^{(n+1)} &= \frac{\mathcal{F}_{ai}^{\mathrm{PHF}} + \sum_{bj}(z_{bj}^{*(n)}\langle ba||ji\rangle + z_{bj}^{(n)}\langle ja||bi\rangle)}{\epsilon_i^{\mathrm{Ref}} - \epsilon_a^{\mathrm{Ref}}},\end{aligned} \tag{34}$$

until $\mathbf{z}^{(n)}$ converges. Once $\mathbf{z}, \mathbf{w}, \mathbf{f}^j$, and $\mathbf{C}$ are obtained, the gradient of the projected energy is given by

$$\begin{aligned}\frac{dE^{j(\mathrm{PAV})}}{dx} = \frac{dL^{\mathrm{PAV}}}{dx} &= W^{\mathrm{PHF}(x)} - E^j\mathbf{f}^{j\dagger}\mathbf{N}^{j(x)}\mathbf{f}^j\\ &+ \sum_{ai}\left[z_{ia}\mathcal{F}_{ai}^{\mathrm{Ref}(x)} + z_{ai}\mathcal{F}_{ia}^{\mathrm{Ref}(x)}\right]\\ &- \sum_{pq} w_{qp}[\mathbf{C}^\dagger\mathbf{S}^x\mathbf{C}]_{pq}.\end{aligned} \tag{35}$$

Finally, with the relaxed and energy-wighted relaxed density matrices

$$\begin{aligned}(\boldsymbol{\rho}_z)_{\mu\nu} &= \sum_{ai}(z_{ai}C_{\nu a}^* C_{\mu i} + z_{ia}C_{\nu i}^* C_{\mu a}),\\ (\boldsymbol{\eta}_z)_{\mu\nu} &= \sum_{pq} w_{qp}C_{\nu q}^* C_{\mu p},\end{aligned} \tag{36}$$

we obtain the energy gradient for the PAV wavefunction,

$$\begin{aligned}\frac{dE^{j(\mathrm{PAV})}}{dx} &= \mathrm{Tr}[\boldsymbol{\rho}_z\mathbf{F}^{\mathrm{Ref}(x)}] - \mathrm{Tr}[\boldsymbol{\eta}_z\mathbf{S}^x]\\ &+ \sum_{mm'} f_m^{j*}f_{m'}^j \sum_g w_g D_{mm'}^{j*}(\hat{R}_g)M_g\left\{E_g^{(x)}\right.\\ &\left.+ (E_g - E^j)\mathrm{Tr}[\mathbf{S}^x\boldsymbol{\rho}_g] - \mathrm{Tr}[\mathbf{F}_g\boldsymbol{\rho}_g\mathbf{S}^x\boldsymbol{\rho}_g]\right\}.\end{aligned} \tag{37}$$

Note that the point group projection requires some additional procedure because the derivative operator with respect to the nuclear coordinate $\partial/\partial x$ does not commute with that for the point group symmetry projection. The detailed derivation is described in the Appendix.

III. COMPUTATIONAL DETAILS

In this section, we apply the analytic energy gradient of PAV-SUHF to methylene, ozone, and the $[Cu_2O_2]^{2+}$ core, in which the nondynamic correlation effects play important roles for their molecular structures. The geometrical optimization was performed starting from the initial geometry optimized at the restricted HF (RHF) or restricted open-shell HF (ROHF). By projecting the BS-UHF wavefunction, we extracted pure singlet and triplet states for $S_z = 0$. There are two possible triplet states by obtained projecting the low-spin BS-UHF ($S_z = 0$) and the high-spin UHF ($S_z = 1$) wavefunctions. We use the notation, e.g., PAV-SUHF ($S_z = 0$) for the spin projected triplet states of BS-UHF ($S_z = 0$). PAV-SUHF and its gradient are implemented into our GELLAN program.[28] The Z-vector equation was solved using the DIIS[25] procedure.

We also performed CASSCF optimizations for comparison. We employed Dunning's correlation-consistent double-zeta basis sets, cc-pVDZ[29–32] for all applications. The Gauss–Legendre quadrature was used for the numerical integration with six quadrature points for spin-projections of BS-UHF.

IV. RESULTS AND DISCUSSION

A. Methylene

One of the most notable successes of quantum chemistry is to predict the bent structure of methylene (CH_2), that is, the simplest carbene. Although the structure of this molecule was believed to be linear from the early experiment of Herzberg, the *ab initio* calculation pointed out that it actually has a bent structure, with H–C–H angle of 133.84°.[33] Now, the ground state of methylene is a radical with two unpaired electrons X^3B_1,[33] described by a configuration of

$$(1a_1)^2(2a_1)^2(1b_2)^2(1b_1)(3a_1).$$

On the other hand, the lowest lying electronic excited state is $\tilde{a}^1A_1$, arising from the closed-shell configuration

$$(1a_1)^2(2a_1)^2(1b_2)^2(3a_1)^2,$$

while the contribution of the double excitation from $3a_1$ to $1b_1$ is importantly large.[34] The triplet state is energetically more favorable than the lowest lying singlet state, so that methylene is a typical case of the RHF instability. The small gap between the singlet and triplet states requires a multireference description, and highly accurate calculations have been performed such as multireference CI (MRCI),[34–39] multireference CC (MRCC),[40–42] and CC singles, doubles, and triples (CCSDT).[34,43]

We carried out the PAV-SUHF geometry optimization of methylene in the singlet and triplet states, to quantify the nondynamic correlation effect by comparing their geometries with those of UHF, CASSCF, and VAP-SUHF. The frontier $1b_1$ and $3a_1$ orbitals were taken as the active orbitals with two electrons for the CASSCF(2,2) calculation and four valence σ orbitals, $2a_1$, $1b_2$, $4a_1$, and $2b_2$ were further included for the CASSCF(6,6) calculation.

The optimized structures and their energies are presented in Table I. We found that the total energies of PAV-SUHF, CASSCF(2,2), and VAP-SUHF are very close to each other within the difference 7 mE_h. In addition, the optimized structures of the singlet state using these three methods are almost the same, in agreement with the experiment. On the other hand, the optimization at the BS-UHF level apparently overestimates the H–C–H bond angle compared with the experiment, although the energy for BS-UHF is lower than those of CASSCF(2,2) and PAV-SUHF. This is explained by the contamination of the stable triplet state in the BS-UHF.

The projection technique is helpful because it clarifies the symmetry-adapted (SA) components. As a result of projection, it is revealed that the BS-UHF state contains two SA states

TABLE I. Optimized structures and energies of methylene in the singlet ($^1A_1$) and triplet ($^3B_1$) states.

	r_{CH} (Å)	a_{HCH} (deg)	E (a.u.)
$^1A_1$			
RHF	1.107	102.75	−38.8811
BS-UHF[a]	1.093	115.62	−38.9030
CAS(2,2)[b]	1.109	102.08	−38.9025
CAS(6,6)[c]	1.139	99.94	−38.9415
PAV-SUHF	1.107	102.86	−38.8980
VAP-SUHF	1.107	103.98	−38.9051
VAP-C_{2v}SUHF	1.135	98.64	−38.9569
Expt.[d]	1.107	102.4	
$^3B_1$			
ROHF	1.081	129.17	−38.9218
UHF[e]	1.081	131.45	−38.9268
CAS(6,6)[c]	1.101	130.98	−38.9606
PAV-SUHF ($S_z = 0$)	1.080	131.85	−38.9232
PAV-SUHF ($S_z = 2$)	1.081	132.24	−38.9296
VAP-SUHF ($S_z = 0$)	1.083	129.22	−38.9268
VAP-SUHF ($S_z = 2$)	1.081	132.24	−38.9326
VAP-C_{2v}SUHF ($S_z = 0$)	1.102	127.44	−38.9629
VAP-C_{2v}SUHF ($S_z = 2$)	1.090	135.25	−38.9603
Expt.[d]	1.075	133.93	

[a]Mixed state of the $^1A_1$ and $^3B_1$ components.
[b]Active space: $3a_1$, $1b_1$.
[c]Active space: $2a_1$, $3a_1$, $4a_1$, $1b_1$, $1b_2$, $2b_2$.
[d]Reference 44.
[e]Mixed state of the $^3B_1$ and $^5B_1$ components.

of equal importance: $|\text{BS-UHF}\rangle = 0.7700|^1A_1\rangle + 0.6373|^3B_1\rangle$. This is consistent with the spin-squared expectation value of $\langle S^2\rangle = 0.8157$. Since the irreducible representation of the pure singlet in BS-UHF is only A_1, the PAV-SUHF projection precisely coincides with the PAV-C_{2v}SUHF one for this system. As shown in Table I, the X^3B_1 methylene has a large bond angle around 130°. Therefore the mixed triplet state gives rise to the large-angle structure. Thus the optimization using BS-UHF is inferior when the contamination is large.

The further energy-lowering from the SUHF level is attained by violating the spatial symmetry of the reference wavefunction and restoring it, namely, by using the VAP-C_{2v}SUHF method. The energy of the optimized structure for VAP-C_{2v}SUHF is 154 mHartree lower than that for the full-valence CASSCF(6,6) method. The bond length and angle only slightly differ between the VAP-C_{2v}SUHF and CASSCF(6,6) approaches; by 0.004 Å and 1.3°, respectively.

The natural orbitals (NOs) for CASSCF(2,2), PAV-, and VAP-SUHF are depicted in Fig. 1. These three give different occupation numbers for $3a_1$ and $1b_1$ NOs, but in principle, they have similar orbital shapes and have a similar pair-like correlation in the occupation numbers between the $3a_1$ and $1b_1$ orbitals. The similarity is also found in the more accurate CASSCF(6,6) and VAP-C_{2v}SUHF calculations, as shown in Fig. 2. While CASSCF(6,6) and VAP-C_{2v}SUHF seem to offer the same quality of results at a glance, there are energetically high-lying 17 NOs that have fractional occupations over 0.001 in the VAP-C_{2v}SUHF calculation, suggesting that the additional correlation effect is gained. This accounts for the lower energy of the VAP-C_{2v}SUHF method than that of CASSCF(6,6).

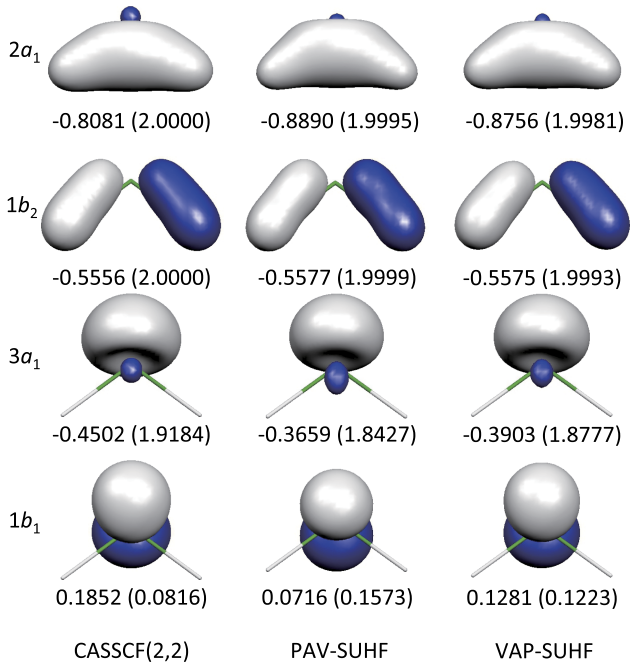

FIG. 1. Natural orbitals for $^1A_1$ state at the CASSCF(2,2), PAV-SUHF, and VAP-SUHF levels of theory. Orbital energies are presented with occupation numbers that are given in the parentheses.

For the triplet state, the optimized bond lengths and angles little depend on the computational methods. The optimized structure using the UHF method and its energy are quite similar to those using ROHF. This is because the spin symmetry of the UHF wavefunction is not violated significantly, as indicated by the spin projection result: $|\text{UHF}\rangle = 0.9980|^3B_1\rangle + 0.0624|^5B_1\rangle$. The PAV approach does not improve the result drastically as long as the spin contamination is small. Actually, the energy and optimized structure of PAV-SUHF are quite similar to the UHF one, and both reproduce the experimental bond length and angle. The VAP scheme provides the total energy lower than PAV by ca. 30 mE_h. The total energy for VAP-C_{2v}SUHF with $S_z = 0$ is the lowest and is comparable to that of CASSCF(6,6) in the triplet state.

B. Ozone

Ozone has been employed as a benchmark system exhibiting a multireference character for the assessment of correlated methods. Its triplet excited states have also been studied extensively since the non-radiative singlet-triplet transition forms a complicated triplet manifold in the near infra-red region, the so-called Wulf band.[45] The electronic structure of the ground state of ozone is singlet, in which two unpaired π electrons at the terminal oxygen atoms form the weakly bound singlet state.[46,47] This leads to the electronic ground state dominated by the configurations, $[\text{core}\cdots](4b_2)^2(6a_1)^2(1a_1)^2$ and $[\text{core}\cdots](4b_2)^2(6a_1)^2(2b_1)^2$. The contribution of these biradical configurations gives rise to the first triplet excited state in $^3B_2$, dominated by the $\pi - \pi^*$ excitation.

We discuss the performance of PHF on the equilibrium geometry of ozone, by comparison with the results from UHF and CASSCF. We performed the CASSCF calculations based on the constructions of active spaces in the C_{2v} point group symmetry in Table II. The optimized structures of ozone using

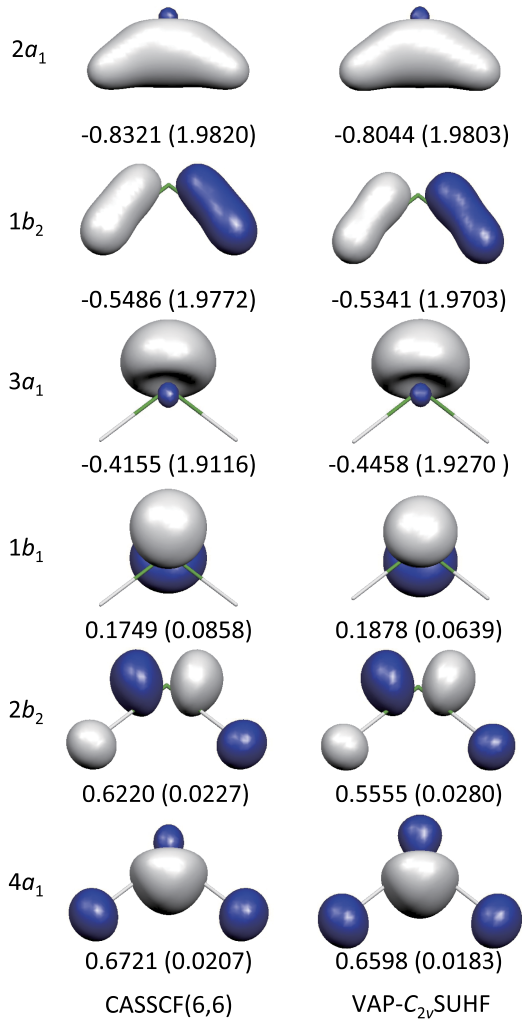

FIG. 2. Natural orbitals for $^1A_1$ state at the CASSCF(6,6) and VAP-C_{2v}SUHF levels of theory. Orbital energies are presented with occupation numbers that are given in the parentheses.

the analytic gradient schemes of PHF along with other electronic structure methods are listed in Table III. RHF underestimates the O–O bond length due to the inability to describe the biradical character. BS-UHF gives a bond length relatively consistent with the experimental one, in contrast to the situation for methylene. However, its bond angle is somewhat smaller than those from other correlated methods due to the contamination of the $^3B_2$ state, which tends to exhibit a longer equilibrium bond length and a smaller angle than those of $^1A_1$. For comparison, the geometrical parameters of ROHF for the $^3B_2$ state are also listed. An analysis using the spin projection reveals the composition of the BS-UHF wave function, $|\text{BS-UHF}\rangle = 0.7272|^1A_1\rangle + 0.4061|^3B_2\rangle$. The

TABLE II. Active orbitals and electrons employed for the CASSCF calculations of ozone.

Method	Orbitals and electrons
CAS(4,3)	$(1b_1)^2(1a_2)^2\ (2b_1)^0$
CAS(6,5)	$(1b_1)^2(6a_1)^2(1a_2)^2\ (2b_1)^0(5b_2)^0$
CAS(8,7)	$(1b_1)^2(4b_2)^2(6a_1)^2(1a_2)^2\ (2b_1)^0(7a_1)^0(5b_2)^0$
CAS(12,9)	$(4a_1)^2(1b_1)^2(5a_1)^2(4b_2)^2(6a_1)^2(1a_2)^2(2b_1)^0(7a_1)^0(5b_2)^0$

TABLE III. Optimized structures and energies of ozone in the singlet ($^1A_1$) and triplet ($^3B_2$) states.

Method	r_{OO} (Å)	a_{OOO} (deg)	E (a.u.)
$^1A_1$			
RHF	1.197	119.006	–224.2806802
BS-UHF[a]	1.290	111.692	–224.3560628
CAS(4,3)	1.244	115.665	–224.3659368
CAS(6,5)	1.240	116.314	–224.3844008
CAS(8,7)	1.290	114.805	–224.4848932
CAS(12,9)	1.290	115.407	–224.4943567
PAV-SUHF	1.260	114.705	–224.3745836
VAP-SUHF	1.275	114.560	–224.3958278
VAP-C_{2v}SUHF	1.269	116.092	–224.5018151
Expt.[b]	1.272	116.78	
$^3B_2$			
ROHF	1.316	108.801	–224.3376347

[a]Mixed state of the $^1A_1$ and $^3B_2$ components.
[b]Reference 48.

PAV optimization provides a reasonable geometry compared with the experiment,[48] due to the exclusion of the unfavorable triplet contaminant. The results from PAV-SUHF and VAP-SUHF are similar to each other. PAV-SUHF gives the state energy in the intermediate quality between CASSCF(4,3) and CASSCF(6,5), providing an appropriate description of the multireference character for this system. It appears that VAP-C_{2v}SUHF recovers most of the nondynamic correlation effects, providing the energy lower than that from CASSCF(12,9) and reproducing the experimental structural parameters.

C. $[Cu_2O_2]^{2+}$

To investigate the performance of the PAV optimization for multinuclear transition-metal systems, we present herein the interconversion profile of the bare $[Cu_2O_2]^{2+}$ core, which has been studied extensively with different theoretical approaches.[7,49–52] As shown in Fig. 3, the schemes $\mu-\eta^2:\eta^2-$ peroxodicopper(II) (**1a**) and bis(μ-oxo)-dicopper(II) (**1b**) are experimentally identified $[Cu_2O_2]^{2+}$ structures. The structures **1a** and **1b** are energetically close with a very low barrier of interconversion.[53–56] However, the multi-reference character changes drastically during the isomerization, and its accurate theoretical description is challenging. The former **1a** is a singlet biradical, where the nondynamic correlation effect is important, while the latter **1b** is even more strongly correlated.[52] Thus, studying the interconversion of $[Cu_2O_2]^{2+}$ core requires a method able to describe the electron correlation in a balanced manner according to a varying degree of biradical character along the isomerization coordinate. The isomerization potential curve of the $[Cu_2O_2]^{2+}$ core has been studied by

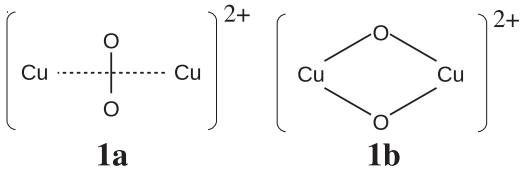

FIG. 3. D_{2h} structures of μ-η^2:η^2-peroxodicopper(II) (**1a**) and bis(μ-oxo)-dicopper(II) (**1b**) in the isomerization profile of the $[Cu_2O_2]^{2+}$ core.

using sophisticated theoretical methods like completely renormalized CC (CR-CC),[49] restricted active-space second order perturbation theory (RASPT2),[50] and DMRG with strongly contracted canonical transformation including only single and double excitations (DMRG-SC-CTSD).[7] A variety of PHF methods has been applied to this system by Samanta *et al.*,[51] and its extension of multi-reference few determinant theory was used by Jiménez-Hoyos *et al.*[52]

We used the isomerization coordinate[49] to describe the potential energy curves (PECs). The nuclear configurations $\boldsymbol{R}$ along the isomerization coordinate f are expressed as

$$\boldsymbol{R} = f\boldsymbol{R}_{\mathbf{1a}} + (1-f)\boldsymbol{R}_{\mathbf{1b}}, \tag{38}$$

where $\boldsymbol{R}_{\mathbf{1a}}$ and $\boldsymbol{R}_{\mathbf{1b}}$ denote nuclear configurations of the model isomers **1a** and **1b**, respectively. The Cu–Cu and O–O distances of **1a** are 3.6 and 1.4 in Å, respectively, and those of **1b** are 2.8 and 2.3 in Å. The previous studies employed the Stuttgart pseudopotential along with the associated basis functions and the atomic natural orbital basis set for Cu and O atoms, respectively. However, we here use the all-electron cc-pVDZ basis set because the profile of the PEC does not change qualitatively at CAS(8,8). The $[Cu_2O_2]^{2+}$ core is eqnarrayed on the yz-plane so that the Cu atoms is on the z-axis, and the eight orbitals mainly originating from Cu $3d$ and O $2p$ orbitals, i.e., $10a_g$, $11a_g$, $5b_{2u}$, $6b_{2u}$, $8b_{1u}$, $9b_{1u}$, $3b_{3g}$, and $4b_{3g}$, are taken as the active orbitals. Note that the PEC profile of CAS(8,8) is quite different from those of higher level of correlated methods like DMRG-SC-CTSD,[7] i.e., CAS(8,8) shows a minimum in the PES which is absent in the results of high-level methods taking dynamic correlation into account.

Fig. 4 shows PECs of RHF, CASSCF, BS-UHF, PAV-SUHF, and VAP-SUHF. To analyze the BS-UHF wavefunction, we performed spin projections onto the SA states with proper spin and point group symmetries in D_{2h}. The

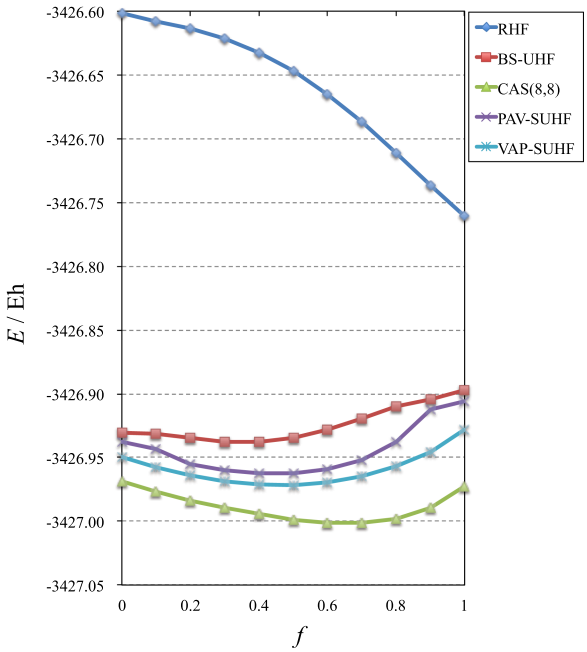

FIG. 4. Isomerization profile of the $[Cu_2O_2]^{2+}$ core using the cc-pVDZ basis set. f indicates the isomerization coordinate (38).

weights of SA components in the BS-UHF wavefunction $\langle P\rangle = \langle \Psi^{\mathrm{BS}}|\hat{P}^{s}_{mm}\hat{P}^{\Gamma}_{\gamma\gamma}|\Psi^{\mathrm{BS}}\rangle$ are depicted as functions of isomerization coordinate in Fig. 5. It is found that the BS-UHF wavefunction at $f = 0$ consists of various SA components in singlet, triplet, and quintet. Accordingly, RHF potentially ineligible to include the necessary spin constituents shows inconsistent PES profile with a high energy at $f = 0$. On the other hand, the BS-UHF state in the $f = 1$ region is described by only two SA state functions: $1/\sqrt{2}(|^1A_g\rangle + |^3B_{3u}\rangle)$, indicating that the nondynamic correlation effects are less pronounced than those in the $f = 0$ region. The PEC of CAS(8,8) shows a minimum in accordance with the previous study.[49] The optimization numerically with respect to the reaction locates the minimum at $f = 0.657$, while the BS-UHF potential minimum is at $f = 0.353$. PAV-SUHF provides a PEC in intermediate quality lying between those of BS-UHF and CAS(8,8) with a minimum at $f = 0.448$. The profile of VAP-SUHF PEC resembles the PAV one with lower energies by 10–30 mE_h and its potential minimum at $f = 0.466$. This is a clear indication that the PAV optimization is as useful as the computationally more demanding one of the VAP scheme.

The multireference character can be measured by the von Neumann entropy,[57]

$$S = -\frac{1}{2}\sum_i \left\{ \frac{n_i}{2}\ln\left(\frac{n_i}{2}\right) + \left(1-\frac{n_i}{2}\right)\ln\left(1-\frac{n_i}{2}\right)\right\}, \tag{39}$$

where n_i denotes the occupation number of natural orbitals. The rate of entropy S/S_{Max} as a function of f is plotted in Fig. 6, where the maximum of the entropy S_{Max} is the value

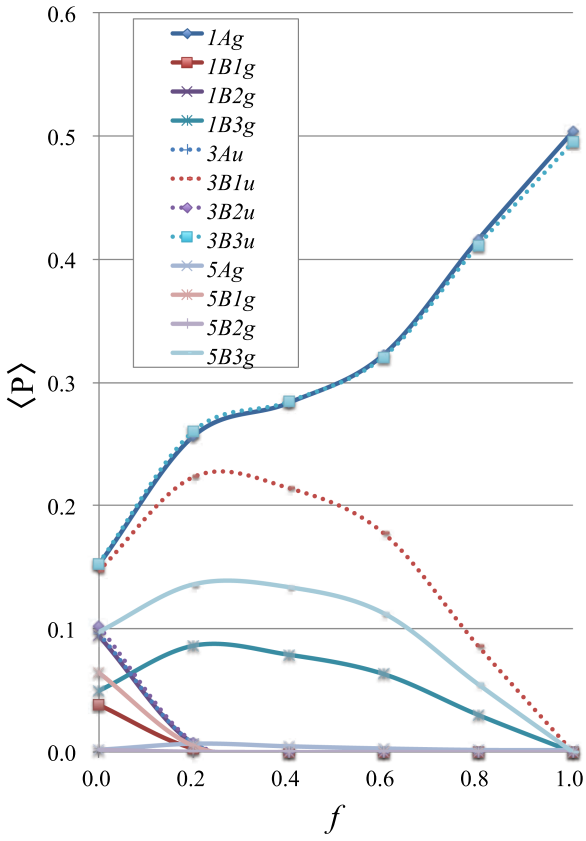

FIG. 5. The weights of symmetry-adapted components from the spin projection of the BS-UHF wavefunction for the $[Cu_2O_2]^{2+}$ core along the isomerization coordinate.

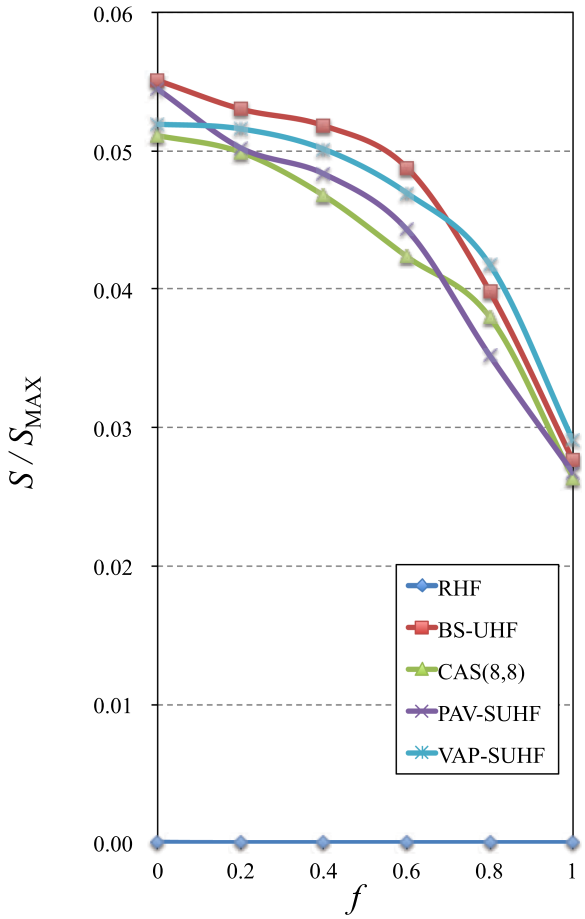

FIG. 6. The von Neumann entropy as a function of the isomerization coordinate f for the $[Cu_2O_2]^{2+}$ core.

of fully entangled state with either $n_i = 1$ or 0. In contrast to the uniform behavior of RHF ($S = 0$), the profiles of BS-UHF resemble those of CAS(8,8) and SUHF methods, indicating that the multireference character of this system is essentially described by BS-UHF. The complexity of the electronic state in the **1b** region ($f \approx 0$) is more pronounced than **1a** ($f \approx 1$). Except for the RHF case, there are four natural orbitals that possess occupations ranging between 0.2 and 1.8 at $f = 0$, while this number decreases to two at $f = 1$. In this way, PAV-SUHF accounts for the most of nondynamic correlation captured by VAP-SUHF.

V. CONCLUSION

The analytic energy gradient of PHF in the PAV scheme is developed as a fast and numerically stable alternative to the VAP scheme. It is shown that the PAV-SUHF scheme provides optimized molecular structures similar to those from VAP-SUHF for methylene, ozone, and the $[Cu_2O_2]^{2+}$ core. The Z-vector equation using the DIIS procedure attains a convergence within 20 iterations in most cases, and this process is much faster than the orbital optimization in the VAP scheme. Therefore, the PAV-SUHF optimization is a useful method with a reasonable computational cost and is likely applicable to large systems where nondynamic correlation is important. Nevertheless, one needs to bear in mind that the PAV scheme leads to a trivial solution when RHF is stable. The dynamic correlation effects sometimes become significantly important in systems like multinuclear transition-metal clusters. We have also developed the analytic energy gradient of the ECISD approach to fulfill this requirement,[22] albeit its application is limited to small molecules due to the large computational cost.

ACKNOWLEDGMENTS

We would like to thank Dr. Yuhki Ohtsuka, Dr. Yu-ya Ohnishi, and Dr. Takashi Tsuchimochi for valuable discussions and helpful comments. This work was supported by MEXT's FLAGSHIP2020 as priority issue 5 (development of new fundamental technologies for high-efficiency energy creation, conversion/storage and use). We are also indebted to the HPCI System Research project for the use of computer resources (Project ID Nos.: hp150228, hp150278).

APPENDIX: ENERGY GRADIENT FOR PROJECTED HARTREE–FOCK METHOD IN TERMS OF POINT GROUP SYMMETRY

1. Force operator

First, we review the definition of the force operator. The force acting on an atom A is given by the gradient of energy with respect to nuclear coordinate $X_{Ar}(r = x, y, z)$,

$$F_{Ar} = -\frac{\partial E}{\partial X_{Ar}}. \tag{A1}$$

The force is described by the combination of the Hellmann–Feynman and Pulay forces

$$F_{Ar} = -\frac{\partial \langle \Psi | \hat{H} | \Psi \rangle}{\partial X_{Ar}} \tag{A2}$$

$$= -\left\langle \Psi \left| \frac{\partial \hat{H}}{\partial X_{Ar}} \right| \Psi \right\rangle - \left\langle \frac{\partial \Psi}{\partial X_{Ar}} \middle| \hat{H} \middle| \Psi \right\rangle - \left\langle \Psi \middle| \hat{H} \middle| \frac{\partial \Psi}{\partial X_{Ar}} \right\rangle. \tag{A3}$$

Therefore the force operator consists of the Hellmann–Feynman and Pulay force operators,

$$\hat{F}_{Ar} = \hat{F}^{(\mathrm{HF})}_{Ar} + \hat{F}^{(\mathrm{P})}_{Ar}, \tag{A4}$$

$$\hat{F}^{(\mathrm{HF})}_{Ar} := -\frac{\partial \hat{H}}{\partial X_{Ar}}, \tag{A5}$$

$$\hat{F}^{(\mathrm{P})}_{Ar} := -\hat{H}\frac{\partial}{\partial X_{Ar}} - \mathrm{H.\,C.}. \tag{A6}$$

Since the force operator is a 1-rank tensor operator, it does not commute with the point group (PG) symmetry projection operator. For this reason, the energy derivative for the PG projection requires additional treatment.

2. Projection of point group symmetry

A PG projection operator onto irreducible representation (irrep) Γ is defined as

$$\hat{P}^{\Gamma}_{\gamma\gamma'} = |\Gamma\gamma\rangle\langle\Gamma\gamma'| \tag{A7}$$

$$= \frac{\dim(\Gamma)}{|G|} \sum_{\hat{R}\in G} D^{\Gamma *}_{\gamma\gamma'}(\hat{R})\hat{R}, \tag{A8}$$

where $|G|$ is the order of the point group G, and $D^{\Gamma}_{\gamma\gamma'}$ stands for the element in the γth row and γ'th column of the representation matrix D^{Γ}, associated with symmetry operation $\hat{R}$. Strictly, $\hat{P}^{\Gamma}_{\gamma\gamma'}$ with $\gamma \neq \gamma'$ is not a projection operator in the mathematical definition but is usually called transfer operator.

In general, the expectation value of energy for the symmetry-adapted (SA) wavefunction is given by

$$E^j_n = \sum_{mm'} f^{j*}_m f^j_{m'} \langle \Psi | \hat{P}^{j\dagger}_{nm} \hat{H} \hat{P}^j_{nm'} | \Psi \rangle. \tag{A9}$$

The energy E^j_n does not depend on n, so we can omit n as $E^j_n = E^j$. True projection operators are commutable with Hamiltonian $[\hat{H}, \hat{P}^j_{mm}] = 0$, Hermitian $\hat{P}^{j\dagger}_{mm} = \hat{P}^j_{mm}$, and idempotent $\hat{P}^j_{mm}\hat{P}^j_{mm} = \hat{P}^j_{mm}$. Likewise, we can derive $[\hat{H}, \hat{P}^j_{mn}] = 0$, $\hat{P}^{j\dagger}_{mn} = \hat{P}^j_{nm}$, and $\hat{P}^j_{kl}\hat{P}^j_{mn} = \delta_{lm}\hat{P}^j_{ln}$ using the great orthogonality theorem. These relations enable us to simplify the energy expression as

$$E^j = \sum_{mm'} f^{j*}_m f^j_{m'} \langle \Psi | \hat{H} \hat{P}^j_{mm'} | \Psi \rangle. \tag{A10}$$

In the case of the spin projection ($j = s$), the energy gradient is also expressed as

$$\begin{aligned} \frac{\partial E^s}{\partial X_{Ar}} = &\sum_{mm'} \frac{\partial f^{s*}_m f^s_{m'}}{\partial X_{Ar}} \langle \Psi | \hat{H} \hat{P}^s_{mm'} | \Psi \rangle \\ &- \sum_{mm'} f^{s*}_m f^s_{m'} \langle \Psi | \hat{F}_{Ar} \hat{P}^s_{mm'} | \Psi \rangle, \end{aligned} \tag{A11}$$

because the force operator is commutable with the projection/transfer operator $[\hat{P}^s_{mm'}, \hat{F}_{Ar}] = 0$. However in the case of the PG projection ($j = \Gamma, m = \gamma', m' = \gamma'', n = \gamma$), we should use two transfer operators

$$\begin{aligned} \frac{\partial E^{\Gamma}_{\gamma}}{\partial X_{Ar}} = &\sum_{\gamma'\gamma''} \frac{\partial f^{\Gamma*}_{\gamma'} f^{\Gamma}_{\gamma''}}{\partial X_{Ar}} \langle \Psi | \hat{H} \hat{P}^{\Gamma}_{\gamma'\gamma''} | \Psi \rangle \\ &- \sum_{\gamma'\gamma''} f^{\Gamma*}_{\gamma'} f^{\Gamma}_{\gamma''} \langle \Psi | \hat{P}^{\Gamma\dagger}_{\gamma\gamma'} \hat{F}_{Ar} \hat{P}^{\Gamma}_{\gamma\gamma''} | \Psi \rangle, \end{aligned} \tag{A12}$$

because the force operator does not commute with the projection/transfer operators. Note that the energy gradient dE^{Γ}_{γ}/dx depends on γ although E^{Γ}_{γ} does not depend on.

3. Wigner–Eckart Theorem

To calculate the energy gradient in the PG projection, we have to use the two projection/transfer operators to act on bra and ket vectors, but it costs great expense to carry out the numerical integration. However, we can reduce the number of projection/transfer operators to one, using the Wigner–Eckart theorem. The force operator is decomposed into 1-rank SA tensor operators

$$\hat{F}_{Ar} = \sum_{\alpha\Gamma\gamma} \hat{T}^{\alpha\Gamma}_{\gamma} u^{\alpha\Gamma\gamma}_{Ar}, \tag{A13}$$

where $\boldsymbol{u}^{\alpha\Gamma\gamma}$ denote normal modes and a set of $\{\boldsymbol{u}^{\alpha\Gamma\gamma}\}$ forms an orthonormal complete system

$$\begin{aligned} \sum_{Ar} u^{\alpha\Gamma\gamma *}_{Ar} u^{\alpha'\Gamma'\gamma'}_{Ar} &= \delta_{\alpha\alpha'}\delta_{\Gamma\Gamma'}\delta_{\gamma\gamma'}, \\ \sum_{\alpha\Gamma\gamma} u^{\alpha\Gamma\gamma *}_{Ar} u^{\alpha\Gamma\gamma}_{Bs} &= \delta_{AB}\delta_{rs}. \end{aligned} \tag{A14}$$

A set of normal modes are obtained by diagonalizing a Hessian. The normal modes can be symmetrized by

$$\boldsymbol{u}^{\alpha\Gamma\gamma} = \frac{\dim(\Gamma)}{|G|} \sum_{\hat{R}\in G} D^{\Gamma*}_{\gamma\gamma}(\hat{R}) \hat{R}(\boldsymbol{u}), \tag{A15}$$

where $\hat{R}(\boldsymbol{u})$ transforms normal modes according to the symmetry operation $\hat{R}$. Using the SA normal modes, the force is decomposed into the SA components

$$F^{\Gamma\gamma;\gamma'\gamma''}_{Ar} = \langle \Psi | \hat{P}^{\Gamma\dagger}_{\gamma\gamma'} \hat{F}_{Ar} \hat{P}^{\Gamma}_{\gamma\gamma''} | \Psi \rangle \tag{A16}$$

$$= \sum_{\alpha\bar{\Gamma}\bar{\gamma}} u^{\alpha\bar{\Gamma}\bar{\gamma}}_{Ar} \langle \Psi | \hat{P}^{\Gamma\dagger}_{\gamma\gamma'} \hat{T}^{\alpha\bar{\Gamma}}_{\bar{\gamma}} \hat{P}^{\Gamma}_{\gamma\gamma''} | \Psi \rangle. \tag{A17}$$

Now, we expand the projection/transfer operators,

$$\hat{P}^{\Gamma\dagger}_{\gamma\gamma'} \hat{T}^{\alpha\bar{\Gamma}}_{\bar{\gamma}} \hat{P}^{\Gamma}_{\gamma\gamma''} = \frac{\dim(\Gamma)\dim(\Gamma)}{|G|^2} \sum_{\hat{R},\hat{R}'\in G} D^{\Gamma*}_{\gamma'\gamma}(\hat{R}) D^{\Gamma*}_{\gamma\gamma''}(\hat{R}') \hat{R} \hat{T}^{\alpha\bar{\Gamma}}_{\bar{\gamma}} \hat{R}'. \tag{A18}$$

Since $\hat{T}^{\alpha\bar{\Gamma}}_{\bar{\gamma}}$ is a 1-rank tensor operator, the transformation according to the symmetry operation $\hat{R}$ is represented by

$$\hat{R} \hat{T}^{\alpha\bar{\Gamma}}_{\bar{\gamma}} \hat{R}^{\dagger} = \sum_{\bar{\delta}} D^{\bar{\Gamma}}_{\bar{\delta}\bar{\gamma}}(\hat{R}) \hat{T}^{\alpha\bar{\Gamma}}_{\bar{\delta}}. \tag{A19}$$

Accordingly,

$$\begin{aligned} \hat{P}^{\Gamma\dagger}_{\gamma\gamma'} \hat{T}^{\alpha\bar{\Gamma}}_{\bar{\gamma}} \hat{P}^{\Gamma}_{\gamma\gamma''} = &\frac{\dim(\Gamma)\dim(\Gamma)}{|G|^2} \sum_{\hat{R},\hat{R}'\in G} \sum_{\bar{\delta}} D^{\Gamma*}_{\gamma'\gamma}(\hat{R}) D^{\bar{\Gamma}}_{\bar{\delta}\bar{\gamma}}(\hat{R}) D^{\Gamma*}_{\gamma\gamma''} \\ &\times (\hat{R}') \hat{T}^{\alpha\bar{\Gamma}}_{\bar{\delta}} \hat{R} \hat{R}'. \end{aligned} \tag{A20}$$

If we define $\hat{R}' = \hat{R^{-1}} \hat{R}''$, the representation matrix for symmetry operation $\hat{R}'$ is represented by the matrix products

$$D^{\Gamma*}_{\gamma\gamma''}(\hat{R}') = \sum_{\delta} D^{\Gamma*}_{\gamma\delta}(\hat{R^{-1}}) D^{\Gamma*}_{\delta\gamma''}(\hat{R}'') \tag{A21}$$

$$= \sum_{\delta} D^{\Gamma}_{\delta\gamma}(\hat{R}) D^{\Gamma*}_{\delta\gamma''}(\hat{R}''). \tag{A22}$$

Therefore, Eq. (A20) is written as

$$\begin{aligned} \hat{P}^{\Gamma\dagger}_{\gamma\gamma'} \hat{T}^{\alpha\bar{\Gamma}}_{\bar{\gamma}} \hat{P}^{\Gamma}_{\gamma\gamma''} = &\frac{\dim(\Gamma)\dim(\Gamma)}{|G|^2} \sum_{\hat{R},\hat{R}''\in G} \sum_{\bar{\delta}\delta} D^{\Gamma*}_{\gamma'\gamma}(\hat{R}) D^{\bar{\Gamma}}_{\bar{\delta}\bar{\gamma}}(\hat{R}) \\ &\times D^{\Gamma}_{\delta\gamma}(\hat{R}) D^{\Gamma*}_{\delta\gamma''}(\hat{R}'') \hat{T}^{\alpha\bar{\Gamma}}_{\bar{\delta}} \hat{R}''. \end{aligned} \tag{A23}$$

Using the great orthogonality theorem

$$\sum_{\hat{R}} D^{\Gamma*}_{\gamma'\gamma}(\hat{R}) D^{\bar{\Gamma}}_{\bar{\delta}\bar{\gamma}}(\hat{R}) D^{\Gamma}_{\delta\gamma}(\hat{R}) = \frac{|G|}{\dim(\Gamma)} \langle \Gamma\gamma | \bar{\Gamma}\bar{\gamma}\Gamma\gamma \rangle \langle \bar{\Gamma}\bar{\delta}\Gamma\delta | \Gamma\gamma' \rangle, \tag{A24}$$

Eq. (A20) is simplified to

$$\begin{aligned} \hat{P}^{\Gamma\dagger}_{\gamma\gamma'} \hat{T}^{\alpha\bar{\Gamma}}_{\bar{\gamma}} \hat{P}^{\Gamma}_{\gamma\gamma''} = &\sum_{\bar{\delta}\delta} \langle \Gamma\gamma | \bar{\Gamma}\bar{\gamma}\Gamma\gamma \rangle \langle \bar{\Gamma}\bar{\delta}\Gamma\delta | \Gamma\gamma' \rangle \hat{T}^{\alpha\bar{\Gamma}}_{\bar{\delta}} \\ &\times \frac{\dim(\Gamma)}{|G|} \sum_{\hat{R}''\in G} D^{\Gamma*}_{\delta\gamma''}(\hat{R}'') \hat{R}'' \end{aligned} \tag{A25}$$

$$= \langle \Gamma\gamma | \bar{\Gamma}\bar{\gamma}\Gamma\gamma \rangle \sum_{\bar{\delta}\delta} \langle \bar{\Gamma}\bar{\delta}\Gamma\delta | \Gamma\gamma' \rangle \hat{T}^{\alpha\bar{\Gamma}}_{\bar{\delta}} \hat{P}^{\Gamma}_{\delta\gamma''}. \tag{A26}$$

We obtain a force formulated with one projection/transfer operator,

$$F_{Ar}^{\Gamma\gamma;\gamma'\gamma''} = \sum_{\alpha\bar{\Gamma}\bar{\gamma}} u_{Ar}^{\alpha\bar{\Gamma}\bar{\gamma}} \langle \Gamma\gamma|\bar{\Gamma}\bar{\gamma}\Gamma\gamma\rangle \sum_{\bar{\delta}\delta} \langle \bar{\Gamma}\bar{\delta}\Gamma\delta|\Gamma\gamma'\rangle \times \langle \Psi|\hat{T}_{\bar{\delta}}^{\alpha\bar{\Gamma}} \hat{P}_{\delta\gamma''}^{\Gamma}|\Psi\rangle. \tag{A27}$$

The matrix elements of the tensor operator is

$$\langle \Psi|\hat{T}_{\bar{\delta}}^{\alpha\bar{\Gamma}} \hat{P}_{\delta\gamma''}^{\Gamma}|\Psi\rangle = \sum_{Ar} u_{Ar}^{\alpha\bar{\Gamma}\delta} \langle \Psi|\hat{F}_{Ar} \hat{P}_{\delta\gamma''}^{\Gamma}|\Psi\rangle. \tag{A28}$$

Finally, we have the force

$$F_{Ar}^{\Gamma\gamma;\gamma'\gamma''} = \sum_{\alpha\bar{\Gamma}\bar{\gamma}} u_{Ar}^{\alpha\bar{\Gamma}\bar{\gamma}} \langle \Gamma\gamma|\bar{\Gamma}\bar{\gamma}\Gamma\gamma\rangle \sum_{Bs} \sum_{\bar{\delta}\delta} u_{Bs}^{\alpha\bar{\Gamma}\bar{\delta}} \times \langle \bar{\Gamma}\bar{\delta}\Gamma\delta|\Gamma\gamma'\rangle F_{Bs}^{\Gamma;\delta\gamma''}, \tag{A29}$$

where

$$F_{Bs}^{\Gamma;\delta\gamma''} = \langle \Psi|\hat{F}_{Bs} \hat{P}_{\delta\gamma''}^{\Gamma}|\Psi\rangle. \tag{A30}$$

Thus we reduce the projection/transfer operators and decompose the force into product of the Clebsch–Gordan coefficients (CGCs) that only depend on the spatial symmetry and reduced matrix elements. This result itself is the statement of the Wigner–Eckart theorem.

4. Energy gradient for point-group-projected Hartree–Fock method

To obtain the Z-vector, we use the Fock matrix of PHF $\mathcal{F}^{\mathrm{PHF}}$ in Eq. (32), and this is expressed as a linear combination of $\mathcal{F}_{\Gamma;\gamma'\gamma''}^{\mathrm{PHF}}$,

$$\mathcal{F}^{\mathrm{PHF}} = \sum_{\gamma'\gamma''} f_{\gamma'}^{\Gamma*} f_{\gamma''}^{\Gamma} \mathcal{F}_{\Gamma;\gamma'\gamma''}^{\mathrm{PHF}}. \tag{A31}$$

Since the Z-vector equation is linear, it is convenient to decompose z into $\mathbf{z}^{\Gamma;\gamma'\gamma''}$ as

$$\mathbf{z} = \sum_{\gamma'\gamma''} f_{\gamma'}^{\Gamma*} f_{\gamma''}^{\Gamma'} \mathbf{z}^{\Gamma;\gamma'\gamma''}. \tag{A32}$$

Then each $\mathbf{z}^{\Gamma;\gamma'\gamma''}$ is obtained from $\mathcal{F}_{\Gamma;\gamma'\gamma''}^{\mathrm{PHF}}$ by solving Eq. (34). The relaxed and energy-weighted relaxed density matrices are also decomposed into

$$\begin{aligned} \boldsymbol{\rho}_z &= \sum_{\gamma'\gamma''} f_{\gamma'}^{\Gamma*} f_{\gamma''}^{\Gamma} \boldsymbol{\rho}_z^{\Gamma;\gamma'\gamma''}, \\ \boldsymbol{\eta}_z &= \sum_{\gamma'\gamma''} f_{\gamma'}^{\Gamma*} f_{\gamma''}^{\Gamma} \boldsymbol{\eta}_z^{\Gamma;\gamma'\gamma''}. \end{aligned} \tag{A33}$$

The relaxed force, which is correction for the PAV scheme, and the force for the VAP scheme are similarly defined,

$$\boldsymbol{F}_{\Gamma;\gamma'\gamma''}^{\mathrm{Relax}} = -\mathrm{Tr}[\boldsymbol{\rho}_z^{\Gamma;\gamma'\gamma''} \mathbf{F}^{\mathrm{Ref}(x)}] + \mathrm{Tr}[\mathbf{S}^x \boldsymbol{\eta}_z^{\Gamma;\gamma'\gamma''}], \tag{A34}$$

$$\boldsymbol{F}_{\Gamma;\gamma'\gamma''}^{\mathrm{VAP}} = -\sum_{\hat{R}_g \in G} D_{\gamma'\gamma''}^{\Gamma*}(\hat{R}_g) M_g \left\{ E_g^{(x)} + (E_g - E^{\Gamma}) \mathrm{Tr}[\mathbf{S}^x \boldsymbol{\rho}_g] - \mathrm{Tr}[\mathbf{F}_g \boldsymbol{\rho}_g \mathbf{S}^x \boldsymbol{\rho}_g] \right\}, \tag{A35}$$

where superscript x means Ar. Using Eq. (A29), we have the energy gradients for the VAP and PAV schemes as follows:

$$\frac{dE_{\gamma}^{\Gamma(VAP)}}{dX_{Ar}} = -\sum_{\gamma'\gamma''} f_{\gamma'}^{\Gamma*} f_{\gamma''}^{\Gamma} \sum_{\alpha\bar{\Gamma}\bar{\gamma}} u_{Ar}^{\alpha\bar{\Gamma}\bar{\gamma}} \langle \Gamma\gamma|\bar{\Gamma}\bar{\gamma}\Gamma\gamma\rangle \times \sum_{\bar{\delta}\delta} \langle \bar{\Gamma}\bar{\delta}\Gamma\delta|\Gamma\gamma'\rangle (\boldsymbol{F}_{\Gamma;\delta\gamma''}^{\mathrm{VAP}}) \cdot \boldsymbol{u}^{\alpha\bar{\Gamma}\bar{\delta}}, \tag{A36}$$

$$\frac{dE_{\gamma}^{\Gamma(PAV)}}{dX_{Ar}} = -\sum_{\gamma'\gamma''} f_{\gamma'}^{\Gamma*} f_{\gamma''}^{\Gamma} \sum_{\alpha\bar{\Gamma}\bar{\gamma}} u_{Ar}^{\alpha\bar{\Gamma}\bar{\gamma}} \langle \Gamma\gamma|\bar{\Gamma}\bar{\gamma}\Gamma\gamma\rangle \times \sum_{\bar{\delta}\delta} \langle \bar{\Gamma}\bar{\delta}\Gamma\delta|\Gamma\gamma'\rangle (\boldsymbol{F}_{\Gamma;\delta\gamma''}^{\mathrm{VAP}} + \boldsymbol{F}_{\Gamma;\delta\gamma''}^{\mathrm{Relax}}) \cdot \boldsymbol{u}^{\alpha\bar{\Gamma}\bar{\delta}}. \tag{A37}$$

Considering the projection of an Abelian point group such as C_{2v}, all the dimensions for irreps are one. CGCs equal one only when $\bar{\Gamma}$ is totally symmetric irrep A_1; otherwise they are zero. Therefore, Eq. (A29) becomes

$$F_{Ar}^{\Gamma\,1;1\,1} = \sum_{\alpha} u_{Ar}^{\alpha A_1} F_{Ar}^{\Gamma;1\,1}. \tag{A38}$$

This force is also obtained by projecting $\boldsymbol{F}^{\Gamma}$ onto the totally symmetric displacement using Eq. (A15). Therefore the energy gradients for the VAP and PAV schemes are simply given by

$$\frac{dE^{\Gamma(VAP)}}{dX_{Ar}} = -|f^{\Gamma}|^2 \sum_{\alpha} \boldsymbol{F}_{\Gamma}^{\mathrm{VAP}} \cdot \boldsymbol{u}^{\alpha A_1}, \tag{A39}$$

$$\frac{dE^{\Gamma(PAV)}}{dX_{Ar}} = -|f^{\Gamma}|^2 \sum_{\alpha} (\boldsymbol{F}_{\Gamma}^{\mathrm{VAP}} + \boldsymbol{F}_{\Gamma}^{\mathrm{Relax}}) \cdot \boldsymbol{u}^{\alpha A_1}. \tag{A40}$$

In this article, we calculated the energy gradients on the basis of Eqs. (A39) and (A40).

[1] C. Møller and M. S. Plesset, Phys. Rev. **46**, 618 (1934).
[2] R. J. Bartlett and M. Musiał, Rev. Mod. Phys. **79**, 291 (2007).
[3] D. Hegarty and M. A. Robb, Mol. Phys. **38**, 1795 (1979).
[4] B. O. Roos, P. Linse, P. E. M. Siegbahn, and M. R. A. Blomberg, Chem. Phys. **66**, 197 (1982).
[5] S. R. White, Phys. Rev. Lett. **69**, 2863 (1992).
[6] G. K.-L. Chan and M. Head-Gordon, J. Chem. Phys. **116**, 4462 (2002).
[7] T. Yanai, Y. Kurashige, E. Neuscamman, and G. K.-L. Chan, J. Chem. Phys. **132**, 024105 (2010).
[8] S. Sinnecker, F. Neese, L. Noodleman, and W. Lubitz, J. Am. Chem. Soc. **126**, 2613 (2004).
[9] K. Yamaguchi, S. Yamanaka, M. Nishino, Y. Takano, Y. Kitagawa, H. Nagao, and Y. Yoshioka, Theor. Chem. Acc. **102**, 328 (1999).
[10] P.-O. Löwdin, Phys. Rev. **97**, 1474 (1955).
[11] A. T. Amos and G. G. Hall, Proc. R. Soc. A **263**, 483 (1961).
[12] S. J. Andrews, D. Jayatilaka, R. G. A. Bone, N. C. Handy, and R. D. Amos, Chem. Phys. Lett. **183**, 423 (1991).
[13] N. C. Handy and J. E. Rice, in *Proceedings of an International Workshop on Quantum Chemistry*, edited by R. Carbo (Elsevier, 1989), Vol. 2, p. 145.
[14] J. Baker, Chem. Phys. Lett. **152**, 227 (1988).
[15] J. Baker, J. Phys. Chem. **91**, 1789 (1989).
[16] Y. G. Smeyers and L. Doreste-Suarez, Int. J. Quantum Chem. **7**, 687 (1973).
[17] P. A. Cox and M. H. Wood, Theor. Chim. Acta. **41**, 269 (1976).
[18] K. Yamaguchi, M. Okumura, and W. Mori, Chem. Phys. Lett. **210**, 201 (1993).
[19] C. A. Jiménez-Hoyos, T. M. Henderson, T. Tsuchimochi, and G. E. Scuseria, J. Chem. Phys. **136**, 164109 (2012).
[20] T. Tsuchimochi and T. Van Voorhis, J. Chem. Phys. **142**, 124103 (2015).
[21] T. Tsuchimochi and T. Van Voorhis, J. Chem. Phys. **141**, 164117 (2014).

[22]T. Tsuchimochi and S. Ten-no, J. Chem. Phys. **144**, 011101 (2016).
[23]T. Tsuchimochi and S. Ten-no, J. Chem. Theory Comput. **12**, 1741 (2016).
[24]R. Schutski, C. A. Jiménez-Hoyos, and G. E. Scuseria, J. Chem. Phys. **140**, 204101 (2014).
[25]P. Pulay, Chem. Phys. Lett. **73**, 393 (1980).
[26]N. C. Handy and H. F. Schaefer, J. Chem. Phys. **81**, 5031 (1984).
[27]F. Furche and R. Ahlrichs, J. Chem. Phys. **117**, 7433 (2002).
[28]A. Gellan, *Hierarchical Quantum Chemistry Program* (Kobe University, 2015).
[29]T. H. Dunning, Jr., J. Chem. Phys. **90**, 1007 (1989).
[30]R. A. Kendall, T. H. Dunning, Jr., and R. J. Harrison, J. Chem. Phys. **96**, 6796 (1992).
[31]A. K. Wilson, T. Mourik, and T. H. Dunning, Jr., J. Mol. Struct.: THEOCHEM **388**, 339 (1996).
[32]D. E. Woon and T. H. Dunning, Jr., J. Chem. Phys. **103**, 4572 (1995).
[33]I. Shavitt, Tetrahedron **41**, 1531 (1985).
[34]C. D. Sherrill, M. L. Leininger, T. J. van Huis, and H. F. Schaefer, J. Chem. Phys. **108**, 1040 (1998).
[35]D. B. Knowles, J. R. Alvarez-Collado, G. Hirsch, and R. J. Buenker, J. Chem. Phys. **92**, 585 (1990).
[36]A. D. McLean, P. R. Bunker, R. M. Escribano, and P. Jensen, J. Chem. Phys. **87**, 2166 (1987).
[37]D. C. Comeau, I. Shavitt, P. Jensen, and P. R. Bunker, J. Chem. Phys. **90**, 6491 (1989).
[38]C. W. Bauschlicher, S. R. Langhoff, and P. R. Taylor, J. Chem. Phys. **87**, 387 (1987).
[39]C. W. Bauschlicher and P. R. Taylor, J. Chem. Phys. **85**, 6510 (1986).
[40]A. Balková and R. J. Bartlett, J. Chem. Phys. **102**, 7116 (1995).
[41]P. Piecuch, X. Li, and J. Paldus, Chem. Phys. Lett. **230**, 377 (1994).
[42]X. Li, P. Piecuch, and J. Paldus, Chem. Phys. Lett. **224**, 267 (1994).
[43]J. D. Watts and R. J. Bartlett, J. Chem. Phys. **93**, 6104 (1990).
[44]P. Jensen and P. R. Bunker, J. Chem. Phys. **89**, 1327 (1988).
[45]O. R. Wulf, Proc. Natl. Acad. Sci. **16**, 507 (1930).
[46]P. J. Hay and T. H. Dunning, Jr., J. Chem. Phys. **67**, 2290 (1977).
[47]M. L. Leininger and H. F. Schaefer, J. Chem. Phys. **107**, 9059 (1997).
[48]T. Tanaka and Y. Morino, J. Mol. Spectrosc. **33**, 538 (1970).
[49]C. J. Cramer, M. Włoch, P. Piecuch, C. Puzzarini, and L. Gagliardi, J. Phys. Chem. A **110**, 1991 (2006).
[50]P. Å. Malmqvist, K. Pierloot, A. R. M. Shahi, C. J. Cramer, and L. Gagliardi, J. Chem. Phys. **128**, 204109 (2008).
[51]K. Samanta, C. A. Jiménez-Hoyos, and G. E. Scuseria, J. Chem. Theory Comput. **8**, 4944 (2012).
[52]C. A. Jiménez-Hoyos, R. Rodríguez-Guzmán, and G. E. Scuseria, J. Chem. Phys. **139**, 204102 (2013).
[53]B. Jung, K. D. Karlin, and A. D. Zuberbühler, J. Am. Chem. Soc. **118**, 3763 (1996).
[54]V. Mahadevan, M. J. Henson, E. I. Solomon, and T. D. P. Stack, J. Am. Chem. Soc. **122**, 10249 (2000).
[55]L. M. Mirica, X. Ottenwaelder, and T. D. P. Stack, Chem. Rev. **104**, 1013 (2004).
[56]L. Q. Hatcher and K. D. Karlin, *Advanced Inorganic Chemistry* (Academic Press, 2006), pp. 131–184.
[57]Z. Huang and S. Kais, Chem. Phys. Lett. **413**, 1 (2005).